Contents lists available at ScienceDirect

Measurement

journal homepage: www.elsevier.com/locate/measurement



Effective visual measurement system for SPT hammer energy measurement

M E Yadhunandan, Panjamani Anbazhagan * 0



Department of Civil Engineering, Indian Institute of Science, Bangalore 560012, India

ARTICLE INFO

Keywords: Standard Penetration Test (SPT) High-Speed Camera (HSC) Visual Measurement Hammer Energy Visual Target Mark Energy Transfer Ratio (ETR)

ABSTRACT

The Standard Penetration Test (SPT) is prone to variability due to complex energy transfer dynamics and equipment inconsistencies. Traditional force and acceleration measurements provide valuable data but fail to fully capture the multidimensional movement of SPT components. Therefore, visual measurements of SPT components using a Line-scan and High-Speed Camera (HSC) with target markers have been attempted, but these are limited to 2-dimensional movements. To address these limitations, this study presents a novel HSC system integrated with circular target markings, offering the measurement of movement of SPT component assembly in all three dimensions and Energy Transfer Ratio (ETR). Controlled laboratory SPT tests were conducted to validate the approach. Experiments were carried out for various range of N-values (N = 5 to R), where vertical displacement corresponds to varying soil relative densities (~15-90 %) and penetration depths (~60-3 mm) for a consistent ~60 % input ETR. ETR was estimated using the proposed method and compared with traditional force and acceleration measurements obtained from the SPT Hammer Energy Measurement Apparatus (SPT-HEMA) at both the anvil and sampler levels. The vertical displacement from HSC matched within \pm 0.1 mm of manual vernier-caliper measurements. The Comparison reveals strong agreement on displacement, velocity, and ETR values for all penetration resistance. The standard error in ETR values between HSC and SPT-HEMA was below 0.5 %. For the same rod length, lower N-values exhibit longer displacement and ETR durations, while higher N-values show shorter displacement duration and concentrated energy dissipation. The proposed approach improves accuracy in SPT dynamics and testing methodologies.

1. Introduction

The Standard Penetration Test (SPT) is a widely used method for subsoil exploration in geotechnical engineering. It is the only in-situ technique that simultaneously provides soil strength and soil samples during testing, enabling the determination of soil type and properties. However, the test is inherently subject to various uncertainties due to the variability in SPT rig equipment and its components, and test practice during testing. These factors contribute significantly to the variability of the SPT N-value, which is a measure of soil resistance to penetration (N value represents the number of blows required to

penetrate the soil sampler into the soil for the last 30 cm out of an overall 45 cm penetration depth). To address these inconsistencies and improve the reliability of the test results, several corrections are applied. Among all corrections, overburden and energy corrections are the most predominant corrections, fulfilling all correction requirements [1,2], as these two account for the influence of soil pressure at the test depth and the energy delivered to the drill rod assembly during the test, respectively.

Accurate measurement of energy transfer during the SPT is crucial for ensuring reliable N values. Previous studies have shown that energy dissipation occurs along the drill rod, affecting energy reaching the split

Abbreviations: SPT, Standard Penetration Test; HSC, High-Speed Camera; ETR, Energy Transfer Ratio; SPT-HEMA, SPT Hammer Energy Measurement Apparatus; fps, Frames Per Second; X, Y, Z, Cartesian coordinates representing three-dimensional movement; MATLAB, Matrix Laboratory software for numerical computing; Nvalue, Number of blows required to penetrate the sampler by 30 cm during SPT; FV Method, Force-Velocity Method for energy calculation; F(t), Time-dependent force (N); V(t), Particle velocity as a function of time (m/s); E, Modulus of elasticity of the material (Pa); A, Cross-sectional area of the rod (m²); c, Wave velocity in the rod material (m/s); Z = EA/c, Impedance of the rod (N-s/m); En(t), Energy at a given time t (J); E_{th} , Theoretical Input Energy from hammer impact (J); E_{th} Standard Error; PIVlab, Particle Image Velocimetry Laboratory (a MATLAB toolbox for image processing); PDA SPT Analyzer, Pile Driving Analyzer SPT Analyzer (a commercially available U.S.-based apparatus for SPT hammer energy measurement); YCbCr model, Luminance-Chrominance Color Space in image and video processing technique.

E-mail address: anbazhagan@iisc.ac.in (P. Anbazhagan).

^{*} Corresponding author.

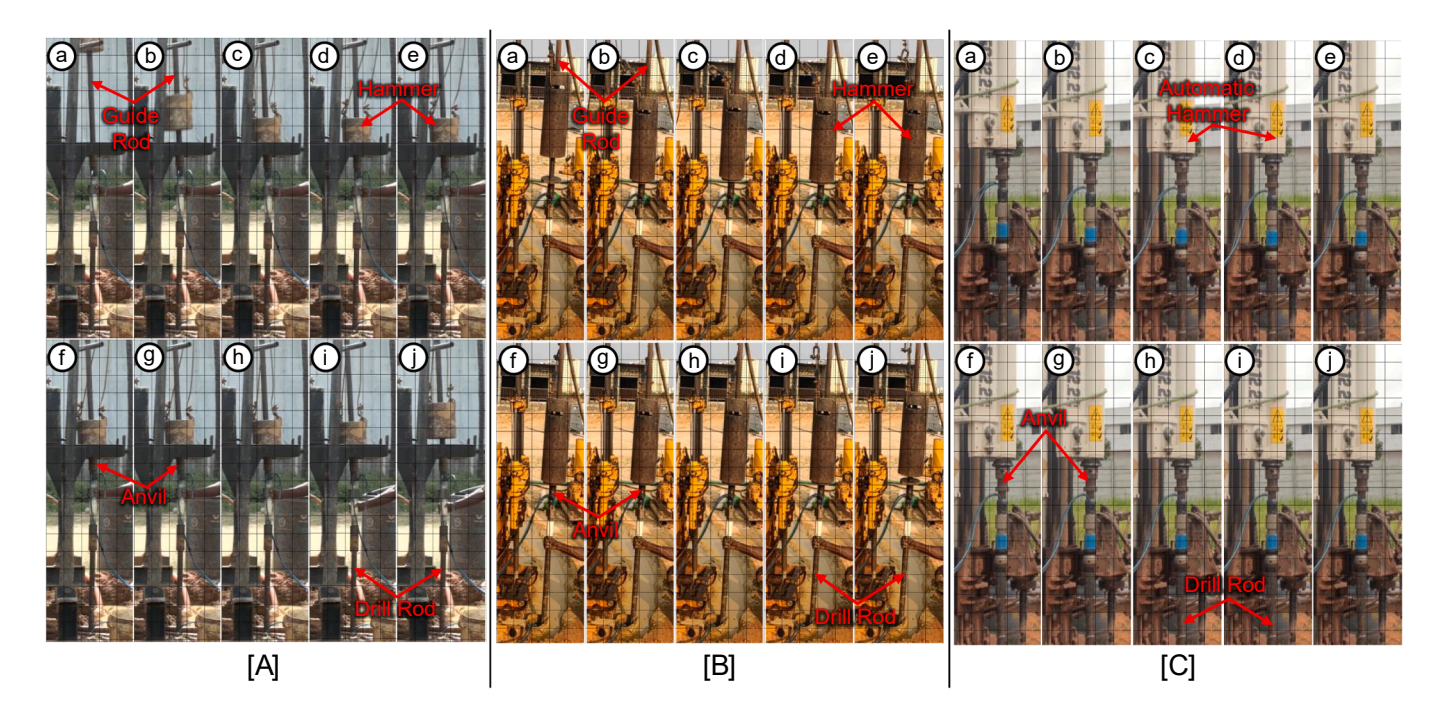


Fig. 1. Typical sequence (a to j) of SPT rod movement and relative position immediately after a hammer blow during SPT test in [A] Rotary Rig, [B] Hydraulic Rig, and [C] Automatic Rig.

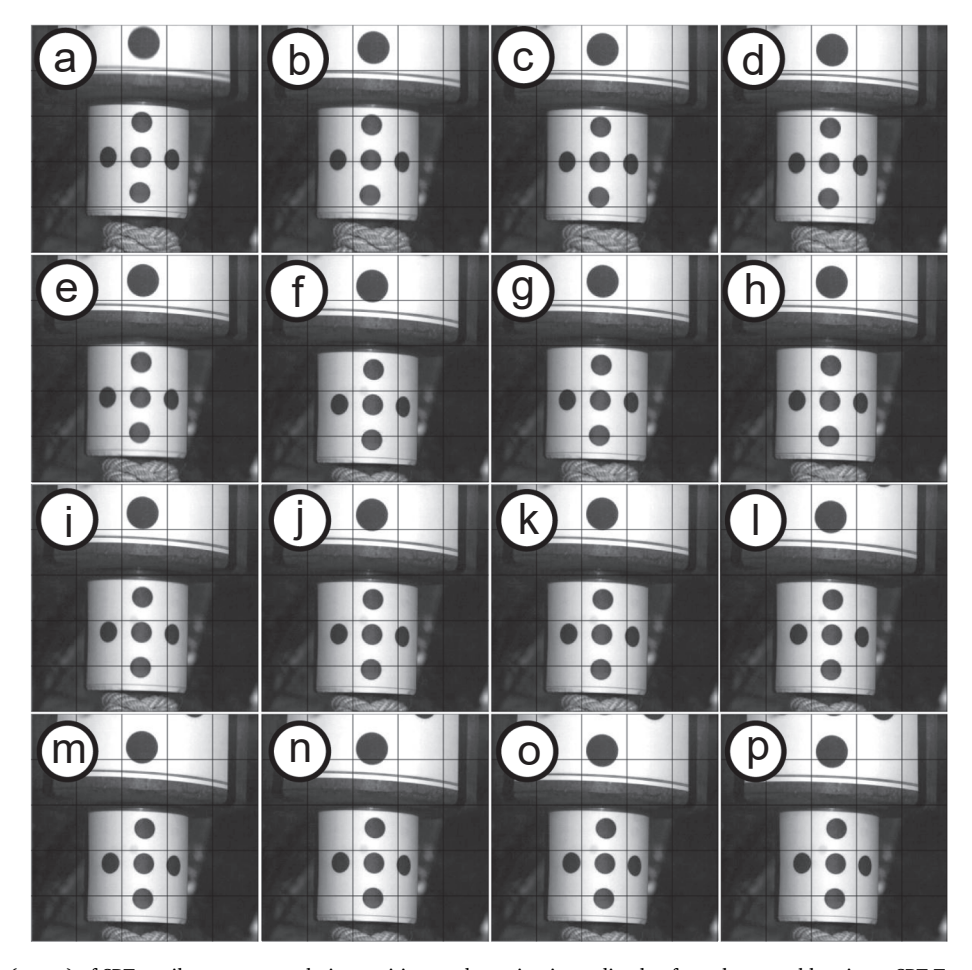


Fig. 2. Typical sequence (a to p) of SPT anvil movement, relative position, and rotation immediately after a hammer blow in an SPT Test, captured using an HSC.

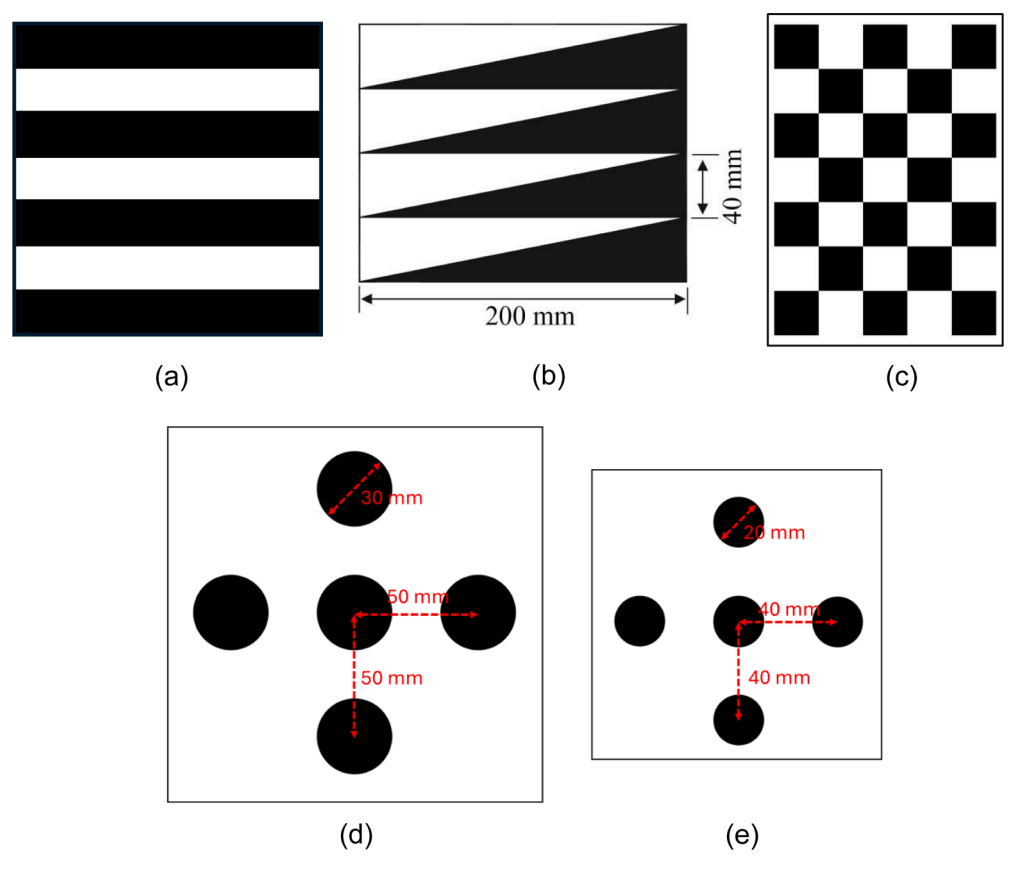


Fig. 3. Typical black and white Target Photographs: (a) Rectangular Strip Shaped Marker, (b) Triangular Strip Shaped Target, and (c) Checkerboard Calibration Pattern; and typical images of the target patterns used in this study: (d) Target picture for the hammer and (e) Target picture for the anvil and sampler.

spoon sampler and highlighted the importance of considering energy measurement at the sampler level rather than just at the anvil level [3]. Generally, the energy measured at the anvil level is considered for evaluating the efficiency of sampler penetration, as it is more accessible for measurement above ground. Hammer energy is estimated using force and acceleration data recorded just below the anvil. This energy is then linked to the N-values, which represent the soil resistance measured at the split-spoon sampler level, located several meters below the surface. From acceleration, velocity is derived, and from velocity, displacement can be calculated. From force and velocity data, the energy efficiency of the hammer impact is calculated using the Force-Velocity method (FV method, [3]). While these measurements provide useful insights, they do not capture the complete picture of the efficiency of sampler penetration. This is because multiple factors influence the behaviour of the drill rod and the resulting N-value. For instance, the vertical alignment of the drill rod plays a critical role, as any deviation from verticality can affect the energy transmission and penetration efficiency. Additionally, the movement of the drill rod after hammer impact, which includes bending, rotation, or lateral displacement of the drill rod assembly, is not easily distinguished through conventional force and acceleration data alone. Furthermore, the depth of sampler penetration per blow varies depending on the N-value. At lower N-values, deeper penetration occurs per blow, whereas higher N-values correspond to shallower penetration, making the energy transfer dynamics highly variable with the soil resistance to penetration. So far, very limited studies have been done to understand the movements of SPT components during hammer impact. To better understand the reasons behind energy loss and variability in N-values, it is important to first observe how SPT components behave during a hammer blow.

1.1. SPT Component Movements

Even though SPT is used in all infrastructural projects, its sophistication in recording and analyzing data is very limited. At the same time, due to the lack of a clear standardization of the parameters of SPT components, local fabrication increased in number, which resulted in several issues during testing [2]. Fig. 1 illustrates sequences (a to j) of the SPT component movements in rotary, hydraulic, and automatic SPT rigs from the field testing. The SPT component movements are captured during the SPT testing using a video camera mounted on a tripod. Movements of the hammer, anvil, and drill rod are noticed in sequential images. Gridline references have been incorporated into each frame of the sequence photographs. This provides visual documentation of the inclination, relative positions and rotations of the SPT components. The movement of SPT components in all directions, as well as the wobbling and rotation of the drill rod assembly, are clearly observable. The rotary rig exhibits the most pronounced movements, characterized by significant wobbling and displacement, as shown in Fig. 1[A]. The hydraulic rig shows comparatively lower movement, yet still evident inclination, vibrations and deviations from the vertical, as shown in Fig. 1[B]. In the automatic rig, movements are further reduced but remain noticeable, as shown in Fig. 1[C]. Even in regular videography, it can be noticed that the automatic SPT rig stabilizes drill rod assembly in the vertical direction but does not eliminate such motions in other directions. In order to study these movements in the controlled environment and also simulate field conditions, an SPT model test setup was set up at the Civil Engineering Department at the Indian Institute of Science (IISc) Bangalore, which is detailed in the further section.

Additionally, the sequence (a to p) of position of SPT components was recorded using a High-Speed Camera (HSC) in a controlled laboratory SPT model setup, as shown in Fig. 2. The figure provides similar observations of hammer and anvil movement during field SPT tests as

Table 1Summary of Literature Review in this study.

Sl No.	Author(s)	Title / Focus	Method used	Key Findings and Limitations
1	Timoshenko & Goodier (1970) [12]	Theory of Elasticity and wave impedance	Elasticity equations for Energy estimation	Impedance relation for energy estimation
2	Santana et al. (2014) [4]	Energy measurement in Brazilian SPT system	Sensors (strain & acceleration)	Energy loss along drill rod, sampler importance, 5 mm accuracy
3	Lim et al. (2002) [6]	Visual measurement using line-scan in pile driving	High-speed line- scan camera	Measured rebound with visual methods
4	Lee et al. (2009) [7]	Effect of secondary impacts on SPT energy	Digital line-scan camera	Captured vertical motion, limited 2D insight
5	Lee et al. (2014) [8]	Real-time monitoring using line-scan camera in SPT	PDA SPT Analyzer + line- scan camera	Real-time monitoring of energy transfer
6	Lee et al. (2002) [5]	Triangular markers for visual tracking in SPT	Triangular & strip markers	Used markers but had distortion issues
7	Zhang (1999) [11]	Flexible camera calibration using a checkerboard	Checkerboard calibration	Enabled distortion correction for cameras
8	Sze et al. (2022) [9]	Visual tracking using graph paper and software	Graph paper + Tracker + PIVlab	2D tracking from video, 1 mm accuracy
9	Miller (2020) [10]	Hammer motion tracking with phone camera	Samsung S9 + camera with scale	Limited frame rate, possible distortion, 1 mm accuracy
10	Kalman (1960) [13]	Kalman filter for dynamic tracking	Kalman filtering algorithm	Predicted circle motion over time
11	Welch & Bishop (1995) [14]	Kalman filter tutorial for motion estimation	Kalman filter theory & practice	Enhanced Kalman filter usage in tracking
12	Comaniciu et al. (2000)	Mean shift for real-time	Histogram- based tracking	Accurate object tracking in videos
13	[15] Bradski (1998) [16]	tracking Face/object tracking for user interfaces	Real-time computer vision tracking	Interface tracking foundations

shown in Fig. 1. The visuals shown in the figure are focused on the hammer and anvil portion for detailed analysis. Unlike the field tests, the laboratory test was conducted in a controlled environment with better control over the rod's verticality and the hammer's free fall. Despite these controls, the images reveal that anvil rotation after the hammer impact and drill rod movement in directions other than the vertical are unavoidable. Such movements are significant as they directly influence the energy transfer from the hammer to the drill rod, reducing the effective energy reaching the sampler. This makes it more challenging to interpret SPT results accurately, as these additional movements disrupt consistent energy delivery and affect measurement reliability.

1.2. Early Attempts in SPT Visual Monitoring

To analyse the complex movements of the drill rod assembly, including the hammer, anvil, and drill rod after the hammer impact, some researchers have investigated the use of visual measurement

techniques during SPT testing. Santana [4] employed a camera in the SPT test without using any target markers, relying instead on a manually held measuring staff to estimate the vertical displacement of the hammer and drill rod. While this approach provided some insight into displacement for each blow, it was significantly limited by the lowresolution measurement markings on the staff, which had the least count of 5 mm. Additionally, maintaining the vertical alignment of the staff by holding manually during testing was challenging. This introduces errors and reduces the reliability of the measurements. This method failed to account for the multidirectional and rotational movements of the drill rod assembly, making it inadequate for a complete analysis of the energy transfer dynamics. Lee et al. [5] and Lim et al. [6] introduced triangular-shaped target photographs (as shown in Fig. 3(a)) for monitoring pile driving analysis using high-speed Line-scan cameras. Building on this concept, Lee et al. [7,8] applied this target marking to monitor hammer and anvil movement during SPT tests using a Line-scan camera. Lee et al. [7] introduced rectangular strip-shaped black-andwhite markers (as shown in Fig. 3(b)) and employed a digital Line-scan camera to capture the vertical movements of the hammer and anvil. This method was specifically designed to capture only the vertical movements of the hammer and anvil during the test. The primary goal was to study the effects of secondary impacts on energy transfer and sampler penetration. Sze et al. [9] and Miller [10] both studied SPT hammer movement using video recordings. They attached graph paper or a scale on the hammer and used 2D motion tracking software like Tracker and PIVlab (Particle Image Velocimetry Laboratory, a MATLAB toolbox for image processing) to measure vertical displacement. The least count in both cases was around 1 mm, limiting the precision of their measurements. Miller recorded video using a Samsung S9 + smartphone, which uses a rolling shutter, not suitable for high-speed motion, leading to possible distortion in fast events like hammer impact. While these approaches provided some valuable insights, their limited ability to measure only vertical movement restricted their overall utility in understanding the full dynamic behaviour of the SPT system. Further, imaging of strip/edge-shaped black-and-white markers on cylindrical shapes can be distorted as the SPT assembly moves in multiple directions. Monitoring these targets can provide data on marker widths and line inclinations, offering some insight into displacement and movement characteristics in 2 dimensions. However, several limitations were encountered, particularly when applying these targets to cylindrical components like the hammer, anvil, and drill rod. The curvature of SPT components causes image distortion of triangular targets and reduces measurement accuracy and reliability. Additionally, for edgeshaped target markings, maintaining a perpendicular line of sight with the camera during testing is challenging. Line-scan cameras were further limited in their capabilities, as they could only measure displacements along the camera's viewing direction, failing to capture multidirectional and rotational movements. Additionally, these studies [7,8] have not included photographic documentation from field tests as part of publications, which restricted the validation and replication of the results. These challenges highlight the need for a more comprehensive approach capable of addressing the full range of movements of SPT components in all directions during field testing.

Checkerboard calibration patterns (as shown in Fig. 3(c)) are widely used for camera calibration purposes [11]. These patterns assist in correcting image distortions such as barrel distortion, pincushion distortion, and fisheye effects. The horizontal and vertical grid structure helps calibrate the camera to ensure accurate footage by referencing geometric corrections. While checkerboard patterns are effective for calibration, they have not been employed in dynamic tests like Pile driving, SPT and Dynamic Cone Penetration Test (DCPT). It can also be noted that square markers tend to distort significantly when applied to cylindrical surfaces, such as those of hammers, anvils, and drill rods. Detecting the edges or corners of squares becomes computationally intensive and prone to inaccuracies when these distortions are introduced. Additionally, identifying the center of a square from distorted

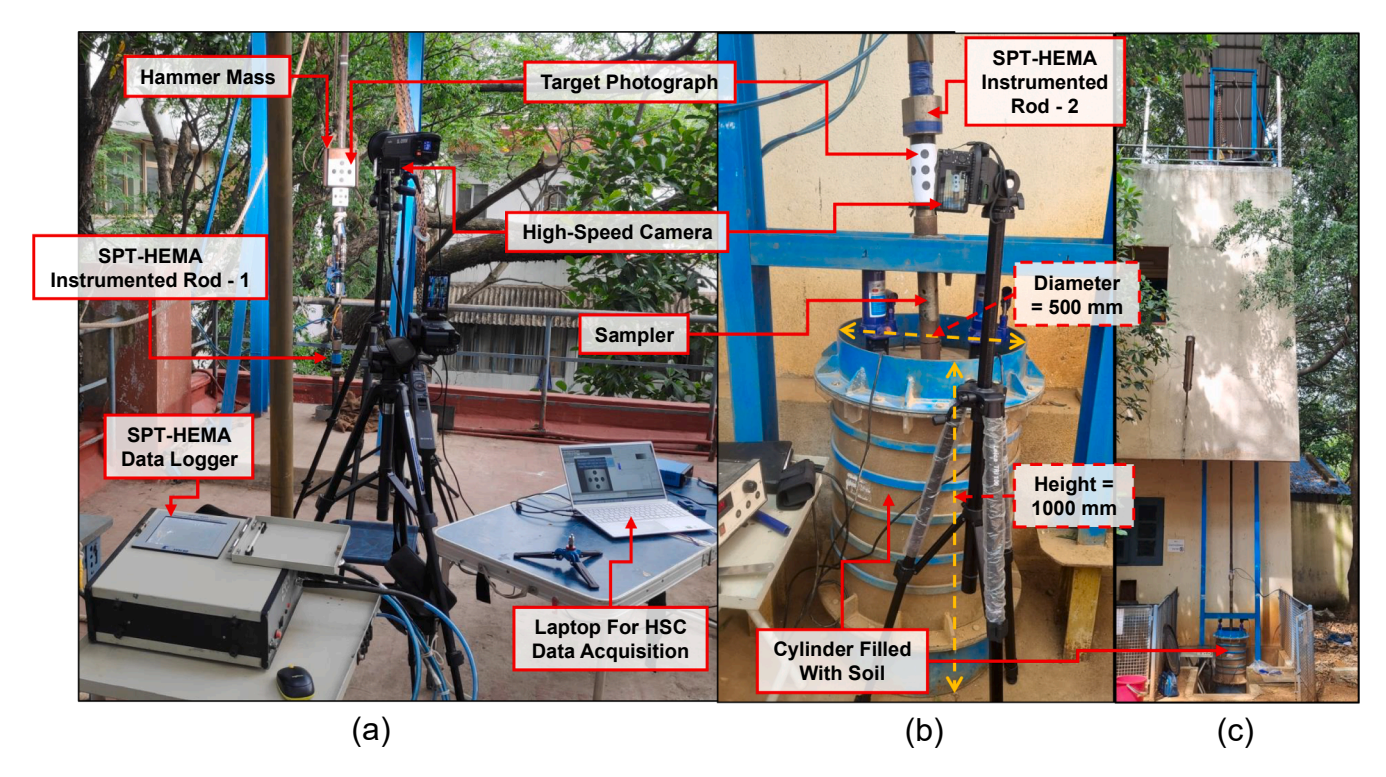


Fig. 4. Laboratory SPT Model setup at IISc and hammer energy measurement using SPT-HEMA with two instrumented rods: Visualized from (a) terrace view, (b) ground floor view, and (c) front view of the building.

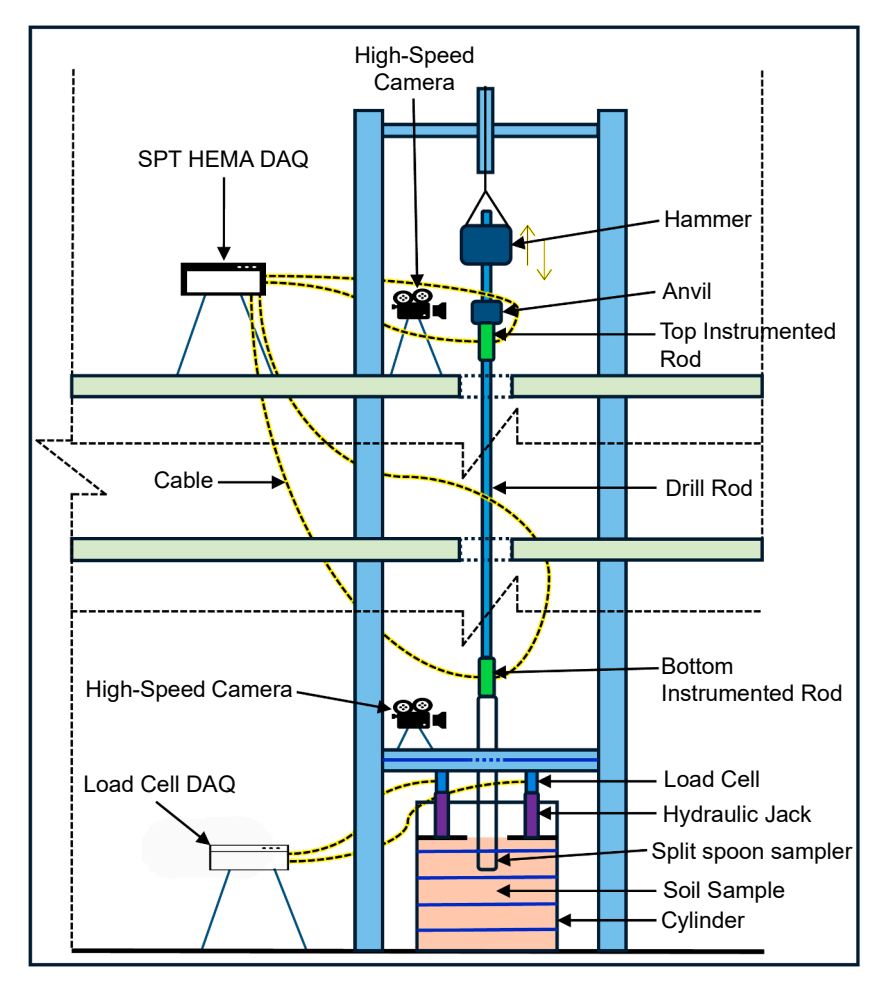


Fig. 5. A schematic sectional view of the SPT laboratory setup at IISc- illustrates the detailed testing arrangement used for the study.

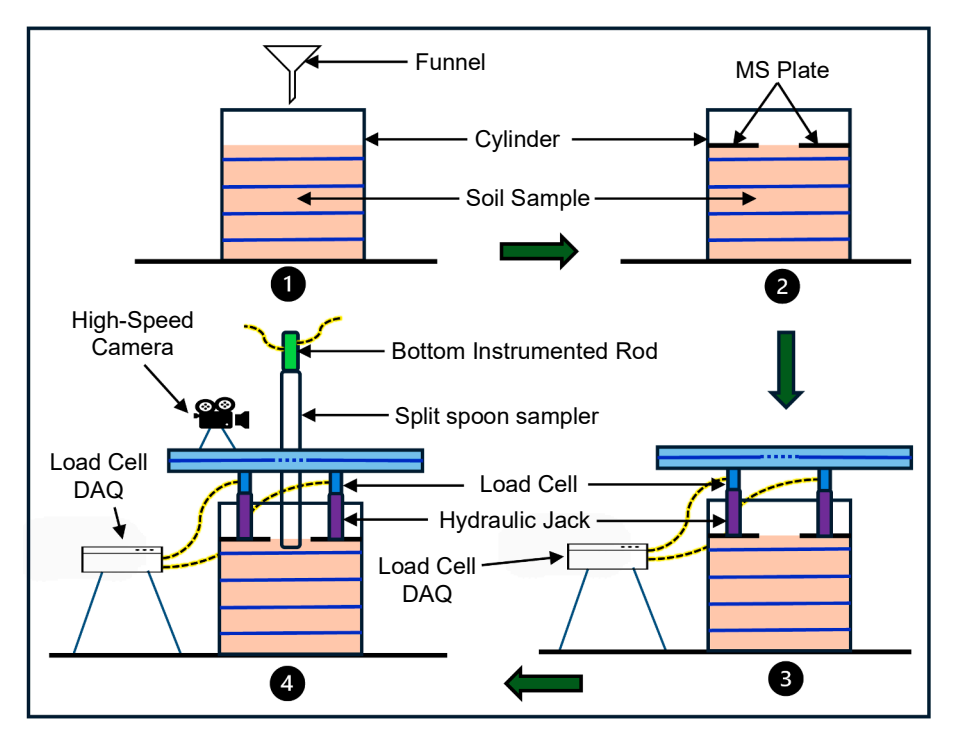


Fig. 6. Schematic representation of the soil filling process in the sampler and the instrumentation arrangement (1 to 4) of SPT-HEMA and HSC within the SPT laboratory setup.

edges is less precise, making it ineffective for accurately tracking rotational movements. Hence, there is a need for an alternative target marker. In this study, circular target markers are used for the first time with HSC systems to monitor the multidirectional movements of SPT components. These inherently adapt better to curved surfaces. This will be explained in detail in the upcoming sections. Additionally, previous research has not fully addressed the variation in penetration resistance across the full range of N-values, from 1 to 100, typically encountered in real soil conditions. Also, there are no comprehensive studies on simultaneous measures of hammer energy and displacement at both the anvil and sampler levels to establish a clear relationship between the Energy Transfer Ratio (ETR) by HSC and conventional testing.

1.3. Summary of Literature Review

Table 1 provides a summary of the studies in the field of SPT energy measurement and visual tracking techniques.

Previous methods using force-acceleration sensors or 2D visual tracking tools mainly focused on vertical motion, offering limited insight into movements in other directions. So far, no study has successfully implemented a 3D visual tracking approach. Hence, in this study, circular target visual measurements were conducted using HSCs, along with sensor-based ETR measurements, to determine displacement and estimate the hammer energy delivered during SPT tests in a controlled full-scale laboratory SPT model setup. These measurements were taken at two key positions: below the anvil, which is the conventional measurement point, and above the split spoon sampler, which is not commonly addressed in existing literature or standardized in codal provisions. The HSC, equipped with a circular target, is capable of capturing the three-dimensional movement of the anvil, hammer, drill rod and sampler during an SPT. Hammer energy estimated using HSC for different soil N-values is compared with conventional hammer energy measurements obtained from force and acceleration data recorded by the SPT Hammer Energy Measurement Apparatus (SPT-HEMA) [1,2]. The HSC with a circular target provides hammer energy estimates comparable to the traditional method. This research contributes to the development of visual measurement systems for hammer energy

estimation in SPT, offering a potential alternative for future geotechnical investigations.

2. Experimental study

2.1. Full-Scale Laboratory SPT Model Test Setup

The controlled full-scale SPT model test setup was built within the existing Soil Mechanics Laboratory building at the Civil Engineering Department, IISc Bangalore. To facilitate the insertion of drill rods and the execution of SPT tests, 150 mm diameter holes have been cut into the floor slabs of the first and second floors. This enables testing to be conducted at various levels, such as the ground floor, first floor, and second floor (terrace), to simulate various drill rod lengths (0.9 to 10 m) and test depths. Fig. 4 shows a multi-perspective view of the laboratory SPT model setup for controlled SPT testing. The figure shows the test arrangement from different viewpoints. Fig. 4(a) shows an overhead view of the entire laboratory setup, the complete layout of measurement and typical data recording. Fig. 4(b) presents a close-up view of the SPT equipment arrangement at the split spoon sampler and soil sample mould. Fig. 4(c) shows the front view of the building, providing a complete view of the laboratory setup and drill rod length. The hammer energy measurements were carried out using the SPT-HEMA developed by Anbazhagan et al. [1,2]. Fig. 5 shows the sectional schematic of the laboratory SPT setup, and the test procedure is explained in the subsequent sections. The SPT-HEMA system with two instrumented rods is used for all data recording. Each rod is capable of recording accelerations up to 10,000 g and loads up to 240 kN. A data logger records the sensor data captured by the instrumented rod at a high sampling rate of 60 kHz for each channel.

Along with SPT-HEMA, two HSCs, namely the 'Pco 1200 hs' and 'Sony DSC-RX100M5A', were used to capture high-resolution video footage of the SPT hammer impact and drill rod assembly movement at the anvil and sampler level. The 'Pco 1200 hs' is a scientific-grade camera, and it is known for its high sensitivity and low noise level video recording. It features a CMOS global shutter sensor and an adjustable aperture of 'f/1.8 to f/16', to prevent motion blur while

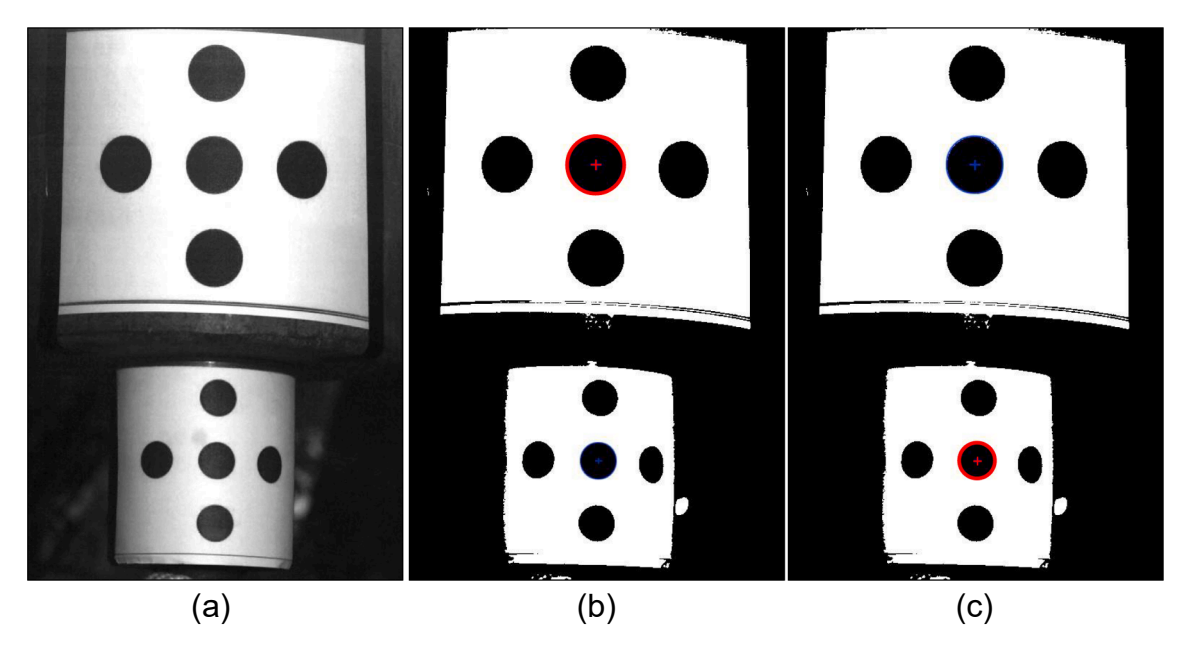


Fig. 7. Typical photograph showing (a) the high-speed camera target pattern attached to the hammer and anvil; and an example of circle tracking using a MATLAB program at the (b) hammer center circle and (c) anvil center circle.

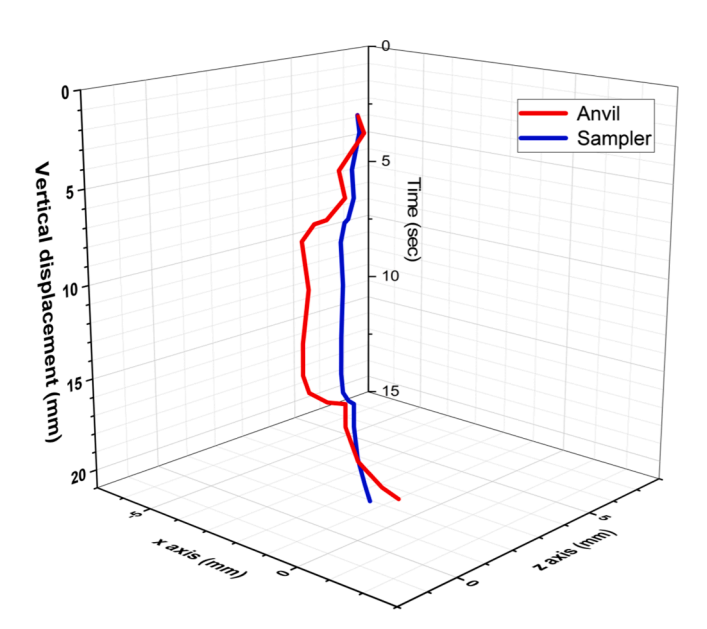


Fig. 8. Typical 3D movement of anvil and sampler after hammer impact.

capturing high-speed motion capturing of an object. The 'Sony DSC-RX100M5A' is a compact high-speed consumer-grade camera. It has a feature of a '1.0-type stacked CMOS sensor' and a 'BIONZ X image processor', which captures high-speed motion with high temporal resolution. It comes with a built-in ZEISS Vario-Sonnar T lens with an aperture range of 'f/1.8 to f/2.8'. The cameras operate at a frame rate of 1087 and 1000 frames per second (fps), generating detailed videos with a resolution of 600x600 and 1244x420 pixels, respectively. This high frame rate and resolution combinations allow for the monitoring rapid movements of the hammer, anvil and drill rod penetration during a hammer impact. The collected data from SPT-HEMA and HSC are processed using custom-developed MATLAB codes. These codes perform essential tasks such as filtering, signal conditioning, and potential feature extraction from the sensor data acquired and the high fps video footage captured by the HSC is used to extract circular target coordinates frame by frame to estimate the SPT component's movement,

displacement, velocity and energy calculations. A detailed explanation of the specific data recording and processing methodologies are explained in subsequent sections.

2.2. Controlled Soil Sample Preparation

Further, as part of the model setup, the soil samples are prepared in a cylindrical drum with a height of 1 m and a diameter of 500 mm. The sand sample is filled in the cylindrical drum in layers (5 to 10 layers). The height of the fall method and tamping are used to achieve the required density of the sand for each layer of fill. Further, the layers were compacted using a vibrator machine to get the required density layerwise, especially for higher density (65 % relative density and above). A 6 mm thick mild steel (MS) annular plate, with an outer diameter of 498 mm and a central opening of 150 mm, is placed on top of the soil sample inside the drum. The 150 mm opening is provided to simulate the borehole diameter commonly used in SPT tests, which typically ranges from 100 mm to 200 mm. Two 5-ton hydraulic jacks connected with 100 kPa load cells apply a vertical load, resembling the overburden pressure experienced during real-world SPT tests. Fig. 6 shows a schematic representation of the soil filling process in the sampler and the instrumentation arrangement of SPT-HEMA and HSC within the SPT laboratory setup. The SPT sampler, drill rod, and hammer assembly strictly adhere to the ASTM D4663 [3] and IS 2131 [17] standards, ensuring consistency with established field practices. To maintain borehole simulations and rod verticality, circular clamps of 150 mm aperture are strategically positioned at every 2-meter interval along the drill rod assembly.

This full-scale model can help to comprehensively characterize the hammer, anvil, and drill rod assembly and sampler dynamics during SPT testing. Since the model setup passes through floor level slab, which enables the use of HSCs recording along with conventional testing. This combined visual measurement approach can facilitate capturing movements of different SPT components that significantly affect energy transfer and sampler penetration efficiency.

2.3. Circular Target Markings in Visual Measurement System

As discussed earlier, the cylindrical shape of SPT components causes distortion of the edge-based targets and does not provide a 3-

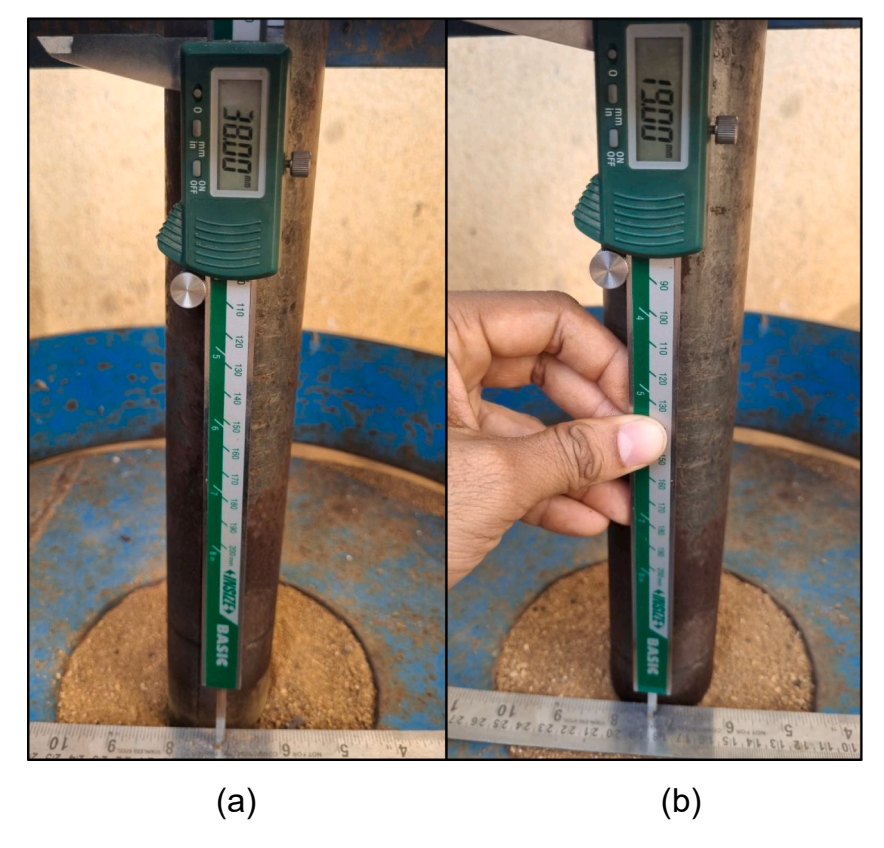


Fig. 9. Vertical displacement measurement for an SPT blow: (a) Before the blow, (b) After the blow.

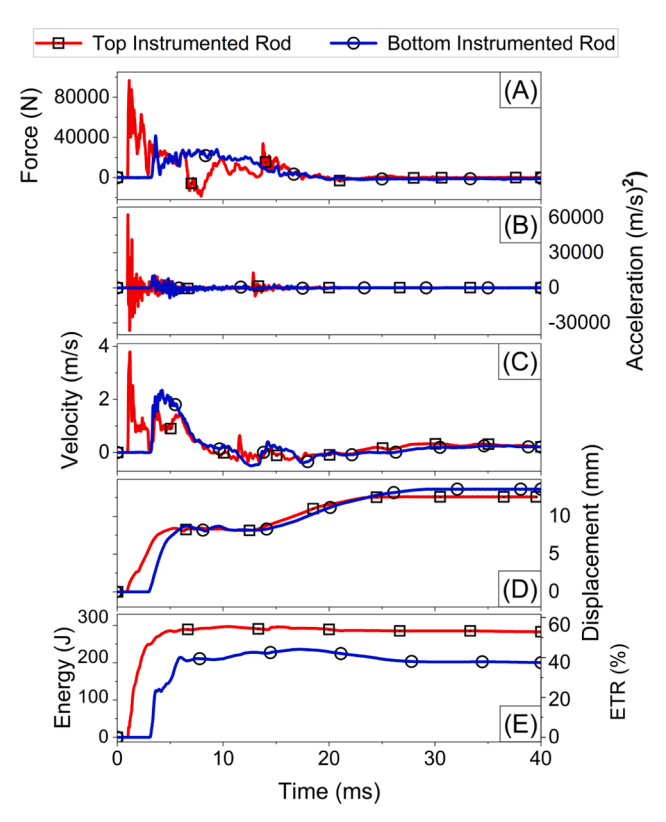


Fig. 10. Typical time history data of (A) Force, (B) Acceleration, (C) Velocity, (D) Displacement and (E) ETR of SPT-HEMA Top and Bottom Instrumented Rod.

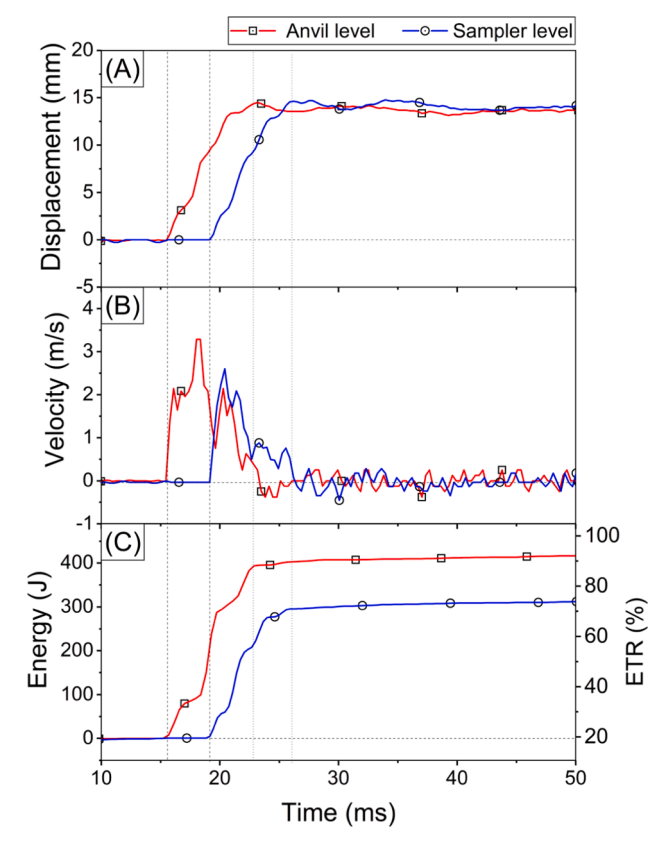


Fig. 11. Typical time history data of HSC at anvil and sampler level: (A) Displacement, (B) Velocity and (C) Energy.

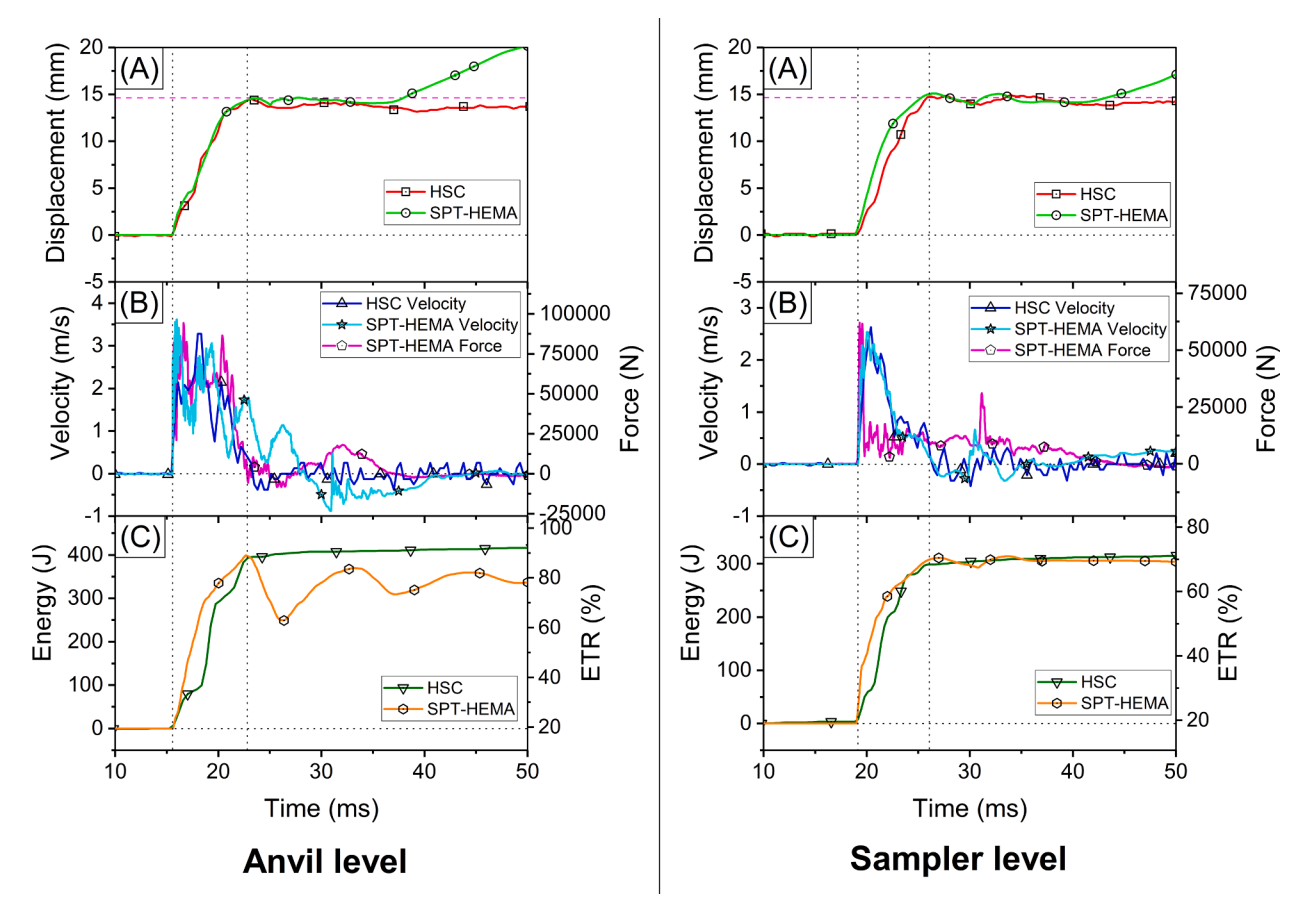


Fig. 12. Typical time history data comparison of SPT-HEMA and HSC at the anvil and sampler level: (A) Displacement, (B) Velocity (with corresponding Force for tension cut-off time information) and (C) Energy.

dimensional overview of displacement. Hence, for the first time, this study employs an HSC system integrated with five circular targets, as shown in Fig. 3. The circular markers are strategically attached to the hammer, anvil, drill rod, and sampler, enabling accurate measurement of movements in all three dimensions (X, Y, and Z coordinates). The system uses custom MATLAB code for image processing, which tracks the circle dimensions and centroid frame by frame.

Using Circular Target marking eliminates the need for strict alignment or precise distance measurements between the camera focal point and the target. This approach uses the pixel data from the camera frame, combined with the actual printed dimensions of the circular markers, for accurate calculations. For instance, the anvil and sampler target features circles with a 20 mm diameter spaced 40 mm apart, while the hammer target uses circles with a 30 mm diameter spaced 50 mm apart, as shown in Fig. 3(d) and Fig. 3(e), respectively. These known dimensions enable the system to reliably track rod movements without relying on external distance measurements or requiring a perfectly perpendicular camera line of sight.

2.4. Target Mark Tracking Technique

This study used two methods to implement visual tracking techniques to analyse circle targets from HSC footage using the MATLAB program. Both methods aim to extract circle coordinates from each frame of the video footage, facilitating accurate displacement and velocity calculations of SPT components. The two approaches are Kalman filter-based tracking [13,14] and histogram-based tracking [15,16].

The Kalman filter is a recursive algorithm for estimating a moving target state with a predictive motion model and measurement updates. In this algorithm, the video footage can be converted to greyscale if

necessary and then the tracking is initiated with a manual selection of the target circle in the first frame of the video, with an interactive bounding box defining the region of interest. The circle boundary under selection is taken as the starting point for the Kalman filter. The algorithm employs a constant velocity motion model for predicting the target position in future frames. For a frame, the location of the circle is predicted in a filter for each frame. The video frame is processed for the computation of the actual circle location with a segmentation function. In case a circle is present, its observation is updated in the Kalman filter prediction; else, in case of obstacles, its predicted location is taken in its place. All frames pass through an iterative algorithm, logging a circle's centre coordinate and circumference pixels for each frame. All information collected is then exported to an Excel file for further analysis.

A histogram-based tracker tracks the circle based on its colour distribution. Like the first method, the video footage can be converted to greyscale if necessary and then the user manually selects the circle in the first frame from the video footage to define the region of interest. The YCbCr model (Luminance-Chrominance Color Space) of colours, in its chrominance channel, is taken for initializing tracking to isolate the circle's salient colour features. In tracking, the chrominance channel of a video frame is taken, and a region of interest is drawn out in the first frame. The region of interest determined by a user is taken for the computation of its histogram. In the following frames, its equivalent is compared for circle position detection. In the case of target loss (a confidence value below a predefined value, in most cases 0.5), an endeavour is taken for re-detecting a circle via a function for segmentation. The circle's position and the detected circle's boundary or circumference are updated, and its centre is calculated. All coordinate values and circle diameters are stored and exported to an Excel file for further analysis.

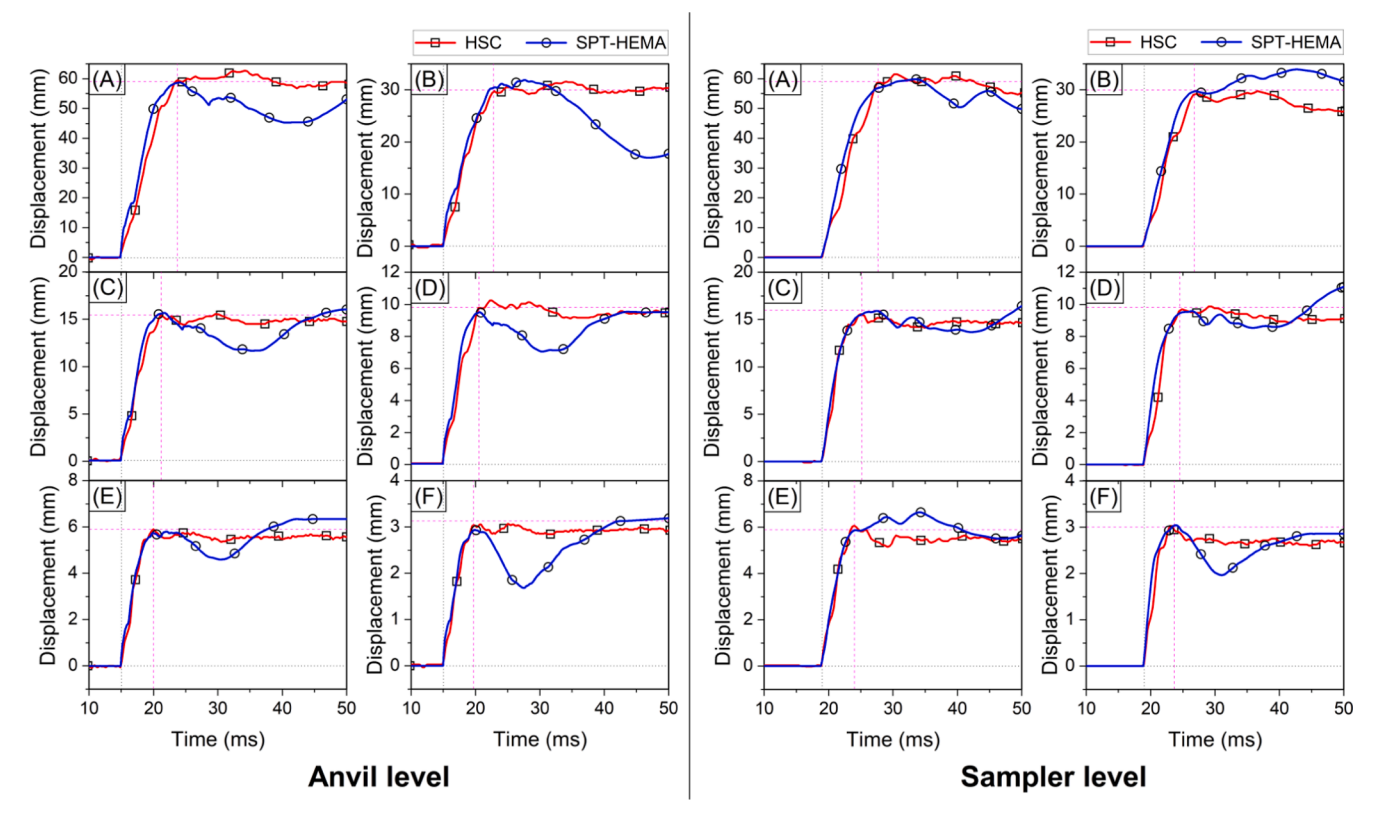


Fig. 13. Typical comparison of Displacement data between SPT-HEMA and HSC at the anvil and sampler level for various N values: (A) N=5, 6 cm penetration per blow, (B) N=10, 3 cm penetration per blow, (C) N=20, 1.5 cm penetration per blow, (D) N=30, 1 cm penetration per blow, (E) N=50, 0.6 cm penetration per blow and (F) $N\sim R$, 0.3 cm penetration per blow.

The Kalman filter is more suitable for cases where motion dynamics are predictable. While the histogram-based tracker is effective for cases with distinctive colour features. Any method or both methods together can be used based on the ambient colour and lighting conditions. Both the Kalman filter-based tracking [18] and histogram-based object tracking [19] have been widely validated in motion analysis and machine vision systems. These works support the accuracy and adaptability of the tracking techniques employed in this study, while the application of circular target tracking is novel. Both methods yielded the same results for tracking circular targets in high-speed video footage frames. The target circles were tracked frame by frame, allowing the calculation of the rod's inclinations and all direction movements. Horizontal inclinations were determined by tracking the relative horizontal distance between the centroids of the circles, while inclinations parallel to the camera axis were obtained by monitoring changes in the target circle diameter. These consistent tracking results across multiple directions demonstrate the reliability of the algorithms. The accuracy of these methods makes them valuable tools for measuring the dynamic behaviour of SPT components.

Fig. 7 shows the typical HSC target patterns and their application in tracking dynamic movements during SPT testing. Fig. 7(a) illustrates the target pattern attached to both the hammer and anvil. Fig. 7(b) and Fig. 7(c) demonstrate an example of a circle track performed at the hammer and anvil centre circles using a custom MATLAB program. The circular markers naturally adapt to the curvature of cylindrical components, such as the hammer, anvil, drill rod, and sampler, which often distorted traditional rectangular or triangular targets used in previous studies. By accommodating curved surfaces, the circular markers ensure consistent and accurate measurements across all directions. The captured changes in the circle's diameter allow for precise tracking of movements towards or away from the camera, enhancing the robustness of the measurement. The system comprehensively captures the SPT

component's vertical displacement, rotation, and inclination by combining analysis of different circle's centroid, X and Y-coordinate movement, and diameter changes.

2.5. Analysis of 3D Movement and Vertical Displacement in SPT

Fig. 8 presents the typical movement of the anvil and sampler in three-dimensional space, recorded using a high-speed camera and circular target markings. This visualisation effectively captures the dynamic behaviour of the SPT components immediately after the hammer impact. From the figure, it is evident that the anvil exhibits significant multidirectional movement, indicating that it undergoes displacement in all three axes (X, Y, and Z). This suggests that not all of the hammer's energy is efficiently transferred to the drill rod. Instead, a portion of the energy is dissipated in lateral and rotational movements of the anvil. This reduces the effectiveness of energy transmission through the drill rod to the sampler. In contrast, the sampler shows a more constrained movement in lateral directions. Since the sampler is embedded in the soil with a seating depth (15 cm), its displacement in lateral directions (X and Z) is significantly lower than that of the anvil. The constrained motion of the sampler ensures that most of the energy transferred from the drill rod is directed towards penetration into the soil rather than being lost in multidirectional movements. These findings help to understand the importance of capturing 3D movement data to assess accurate energy transfer efficiency during the SPT. This approach overcomes the limitations of previous methods using earlier target markers by accurately recording the multidirectional movement of SPT components. Unlike earlier techniques that primarily captured vertical displacement, the current method allows for a more comprehensive understanding of energy dissipation and transfer in all three directions.

Fig. 9 illustrates the vertical displacement measurement taken before and after an SPT blow. A vernier-caliper is used to record the

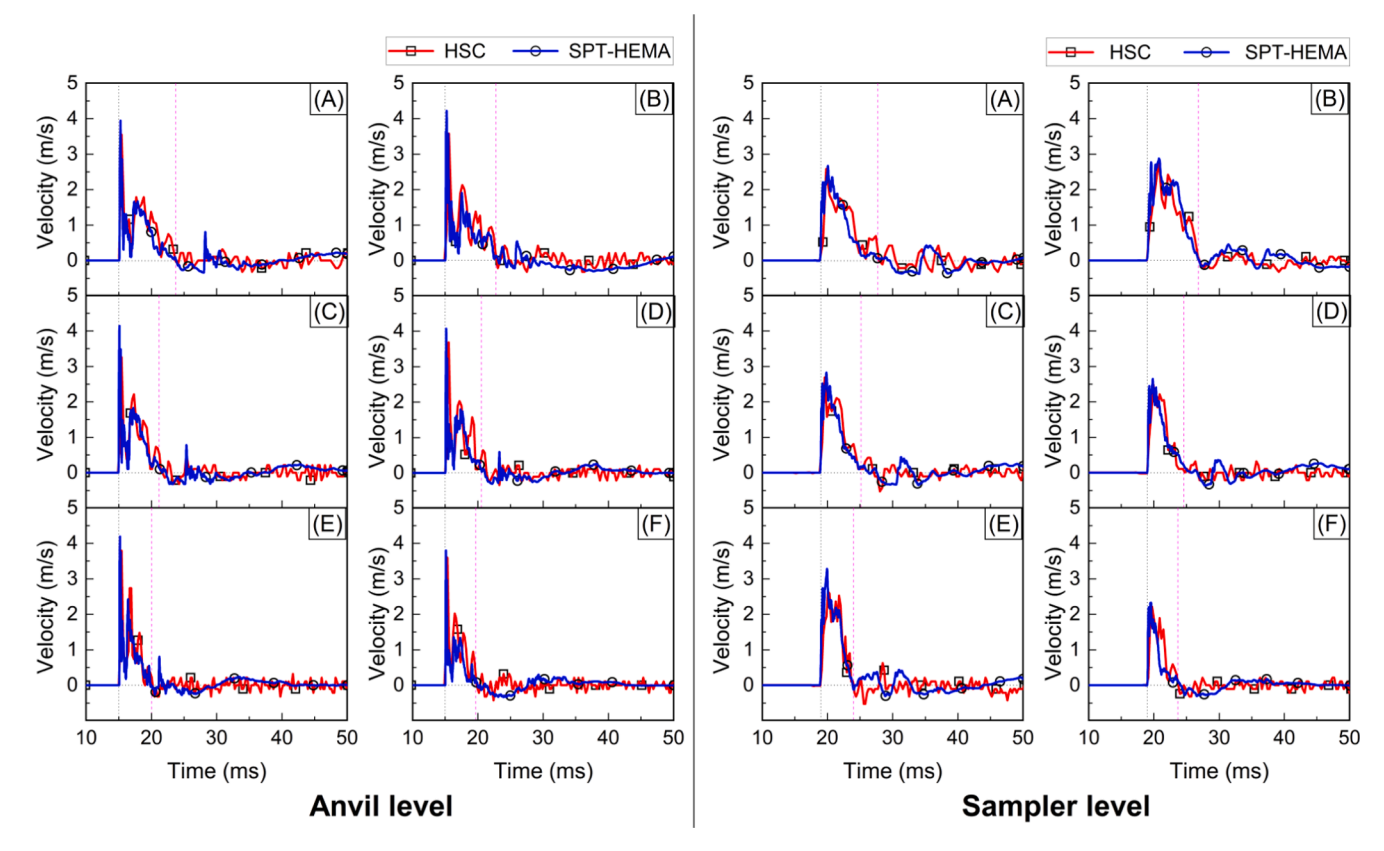


Fig. 14. Typical comparison of Velocity data between SPT-HEMA and HSC at the anvil and sampler level for various N values: (A) N = 5, 6 cm penetration per blow, (B) N = 10, 3 cm penetration per blow, (C) N = 20, 1.5 cm penetration per blow, (D) N = 30, 1 cm penetration per blow, (E) N = 50, 0.6 cm penetration per blow and (F) $N \sim R$, 0.3 cm penetration per blow.

displacement at both stages. These measurements are taken for each blow to ensure accurate tracking of displacement. In the example shown, the displacement recorded using the vernier-caliper is 19 mm. This value is the same as the vertical displacement obtained from the high-speed camera, which also measures 19 mm at both the anvil and sampler levels, as shown in Fig. 8. This comparison confirms the reliability of the high-speed camera method in accurately capturing SPT component displacement. The details of the analysis and measurements are discussed further in the upcoming sections of the study.

In the current study, the analysis focused exclusively on the vertical movements by tracking the y-coordinates of the centroids. This approach ensured that the calculated displacements and energy were confined to the vertical component, which directly impacts the sampler penetration in the SPT. While other motions, such as rotations and nonvertical movements of the drill rod assembly, were also measured, they are not included in this study as they do not contribute to the vertical penetration of the sampler and fall outside the scope of this research. The obtained vertical displacement results are then compared with the SPT-HEMA results and manual displacement measurements taken before and after the SPT blow using a vernier-caliper, which is discussed in detail in the subsequent sections.

2.6. ETR Estimation from HSC Displacement

A systematic method is followed to calculate energy transfer from the vertical displacement data obtained from the HSC. First, the velocity is derived from the displacement measurements through numerical differentiation. The two-point velocity averaging method is then applied to reduce noise and smoothen the velocity values for improved accuracy. These velocity values are subsequently used to calculate the energy transfer during the SPT.

The energy transfer, En(t), can be calculated using the relationship

between force and velocity, as defined in SPT testing standards [3]. The energy equation is represented as shown in Equation (1).

$$En(t) = \int F(t)V(t)dt \tag{1}$$

here, En(t) is the energy at a given time t, F(t) is the time-dependent force, and V(t) is the particle velocity.

For wave propagation in a uniform, unsupported elastic rod, the relationship between proportional force and velocity can be simplified using the concept of rod impedance. According to Timoshenko and Goodier [12], this relationship is represented as shown in Equation (2)

$$F(t) = V(t)(EA/c) (2$$

where, E is the modulus of elasticity, A is the cross-sectional area, c is the wave velocity in the material, EA/c is the impedance (Z) of the rod. Using this proportionality, the energy at a point in the rod can also be expressed entirely in terms of velocity as shown in Equation (3).

$$En(t) = (EA/c) \int_0^t V^2(t)dt$$
 (3)

This formulation simplifies energy calculation by requiring only velocity measurements. The velocity, derived from the displacement data, is squared, and integrated over the time window corresponding to the first compression pulse, which represents the primary energy transfer phase. By focusing on velocity-based calculations, the energy estimation becomes more robust and less sensitive to the complexities of multidirectional vibrations that can affect force measurements and ensure accurate energy transfer estimation.

Furthermore, the ETR can be determined using Equation (4), which is calculated as the ratio of the measured energy En(t) to the theoretical input energy from the hammer impact (which is derived from the

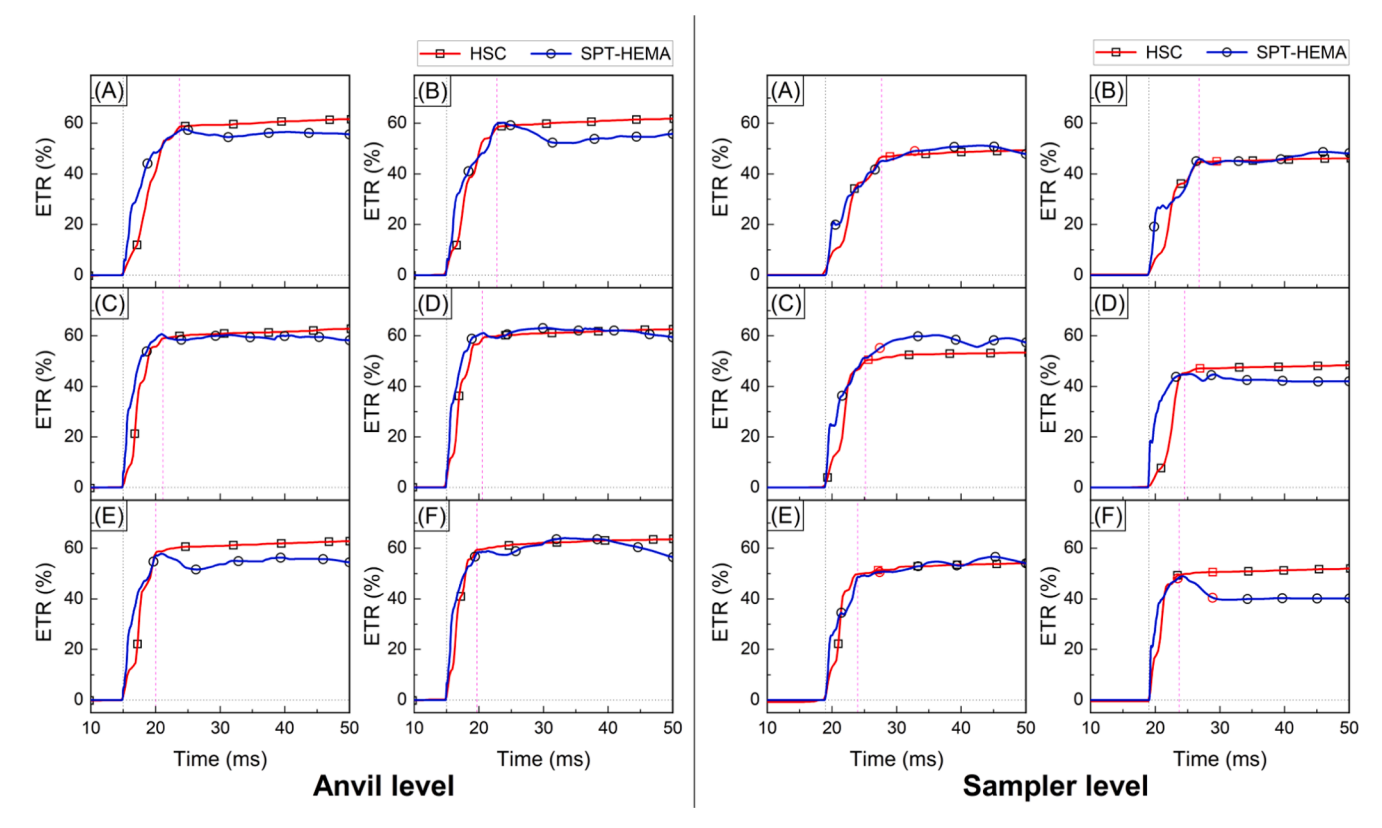


Fig. 15. Typical comparison of ETR data between SPT-HEMA and HSC at the anvil and sampler level for various N values: (A) N = 5, 6 cm penetration per blow, (B) N = 10, 3 cm penetration per blow, (C) N = 20, 1.5 cm penetration per blow, (D) N = 30, 1 cm penetration per blow, (E) N = 50, 0.6 cm penetration per blow and (F) N = 10, 0.3 cm penetration per blow.

product of the hammer weight and its drop height).

$$ETR(\%) = (En(t)/E_{th})100\%$$
 (4)

3. Results and discussion

3.1. Experimental Results

The field equipment undergoes more complex multidirectional movements, as evident in the photograph (Fig. 1), which need to be accounted for in SPT N values correction. As multidirectional movement can result in energy loss, estimating energy only below the anvil may not be sufficient. Hence, a controlled laboratory SPT model setup is used for the comparison of HSC and SPT-HEMA energy variation at the below anvil and above split spoon sampler. Systematic experiments were conducted using the SPT model setup at IISc to evaluate how the ETR derived from the HSC recordings compares with conventional hammer energy measurement practices.

Fig. 10 shows the time history data measured during an SPT using the SPT-HEMA system, highlighting differences between the top and bottom instrumented rods. Fig. 10(A) shows force, with sharp spikes at the top rod due to hammer impact, followed by attenuation as the wave propagates to the bottom rod, indicating energy loss along the rod. This attenuation of energy is consistent with the findings from previous studies [20,21,22]. Fig. 10(B) displays acceleration, where high-frequency oscillations are more prominent at the top, reflecting dissipation during wave travel. Fig. 10(C) illustrates velocity profiles derived from acceleration, with rapid increases and decay at the top rod and delayed responses at the bottom due to wave travel time. Fig. 10(D) shows displacement derived from velocity, with the top rod initially exhibiting higher displacement, which equalizes at the bottom rod after wave propagation. Fig. 10(E) presents the ETR, showing a higher initial ETR that stabilizes as energy is transferred downward. Such

measurements align with prior research that has evaluated the driving energy transferred to split spoon samplers, highlighting the importance of accurate energy measurement techniques in SPT [21]. The differences between the top and bottom rods highlight energy losses caused by factors like energy dissipation, rod vibrations, joints, verticality, misalignment, etc.

Fig. 11 shows the time history data obtained from the HSC system using circular target markers. The figure illustrates the vertical displacement, velocity, and energy at both the anvil and sampler levels. The recorded video footage was processed and analysed using MATLAB program, enabling precise tracking and measurement of the target movements. In Fig. 11(A) the vertical displacement at the anvil and sampler levels is shown. The displacement at both levels reaches the same peak value, confirming a consistent displacement pattern. However, a time lag is observed between the anvil and sampler levels, corresponding to the time taken for the stress wave to travel from the anvil to the sampler through the drill rod assembly obtained from SPT-HEMA sensor recording. Fig. 11(B) illustrates the velocity profiles at the anvil and sampler levels. The velocity at the anvil shows an earlier peak, which aligns with the displacement behaviour and reflects the propagation of the stress wave. Fig. 11(C) shows the energy calculated at both levels using the obtained velocity data (using Equation (3)), highlighting the gradual energy transfer from the hammer impact at the anvil to the sampler level.

Fig. 12 compares the typical time history data of a hammer blow collected from the SPT-HEMA system and the HSC at the anvil and sampler levels. The plots illustrate vertical displacement, velocity (with force for tension cut-off information), and energy. In Fig. 12(A), the vertical displacement profiles of SPT-HEMA and HSC align closely at both anvil and sampler levels, particularly during the critical time window where the displacement reaches its peak. This time window represents the point of maximum energy transfer from the hammer to

the drill rod or sampler, confirming the reliability of both systems in capturing the critical dynamics of vertical motion. However, after 40 ms, a small rise in displacement is seen in the SPT HEMA results. This rise after the peak is likely to be due to signal noise or small vibrations in the rod. It may be caused by leftover wave reflections or slight force changes sensed by the load cell. Fig. 12(B) compares velocity profiles, supplemented by force data to highlight tension cut-off points. The velocity profiles from both systems match well up to the peak displacement at both anvil and sampler levels, showcasing consistent behaviour. Beyond the peak, the SPT-HEMA velocity shows minor deviations, transitioning to negative values and stabilizing, while the HSC velocity remains close to zero with minimal oscillations. Fig. 12(C) compares the energy profiles from both systems, with a strong match observed during the time window of peak displacement at both the anvil and sampler levels. The energy values during this phase reflect the maximum energy transfer, which is the primary focus of the analysis. Beyond the peak displacement, minor differences in energy profiles arise due to variations in force and velocity data, with SPT-HEMA exhibiting oscillation and HSC maintaining stability. This is due to wave reflections and vibrations in the rod. These include compressive and tensile waves bouncing at joints and boundaries. Since energy is calculated using both force and velocity, even small changes in these signals cause variations. Unlike the smoother displacement-based HSC method, SPT-HEMA records dynamic signals of force and acceleration, that are more sensitive to noise and reflections. However, these variations beyond the critical window are less relevant. The results highlight the importance of analyzing energy values during the time window corresponding to peak displacement, as it represents the most significant phase of energy transfer for sampler penetration. The consistent agreement between SPT-HEMA and HSC during this critical phase demonstrates their accuracy in capturing energy transfer dynamics, ensuring reliable interpretations of SPT results.

3.2. ETR Comparison for Different Soil States

In order to understand the performance of HSC with circular targets for different states of soil, tests are performed for different relative densities (\sim 15–90 %) of soil. The relative density of soil represents the number of blows required to achieve specific penetration depths, corresponding to varying energy levels. During these tests, an energy level of around 60 % is maintained for consistency, and then the displacement, velocity and ETR are compared. The samples are prepared in the cylinder with uniform density throughout the soil fill depth, as described earlier. From test records, N-values analyzed include N = 5 (6 cm/blow), N = 10 (3 cm/blow), N = 20 (1.5 cm/blow), N = 30 (1 cm/blow), N = 50(0.6 cm/blow), and N \approx R (0.3 cm/blow). Fig. 13 to Fig. 15 present the displacement, velocity, and ETR comparisons, respectively, at both the anvil and the sampler levels. In the plotted results, the horizontal black dotted line represents the zero-reference line, while the vertical black dotted line marks the starting point time of the arrival of a stress wave due to a hammer blow. At the anvil level, this point appears earlier, whereas at the sampler level, it is delayed due to the time required for the stress wave to travel from the anvil to the sampler. Additionally, the vertical dashed magenta colour line indicates the duration or the point, where the peak displacement value occurs. The maximum ETR was determined based on the corresponding peak displacement point, ensuring consistency in energy estimation at both measurement levels.

The displacement data, as shown in Fig. 13, exhibit strong agreement between the SPT-HEMA and HSC measurements across all N-values at both the anvil and sampler levels. For lower N-values (e.g., N=5 and N=10), which correspond to greater penetration per blow, the time required to achieve peak displacement is longer. Conversely, for higher N-values (e.g., N=50 and $N\approx R$), the penetration per blow is smaller, resulting in shorter times to reach peak displacement. This trend is observed at both the anvil and sampler levels. Additionally, the displacement measurement for each blow, both before and after the SPT blow, is manually recorded using a vernier-caliper, as mentioned earlier.

These manually measured values are incorporated into the plots as horizontal dashed lines in magenta colour. A strong match is observed between the manually recorded values and the maximum displacement obtained from both the high-speed camera and the SPT-HEMA system. Despite the variations in time to reach peak displacement across N-values, the peak displacement magnitudes from both systems align closely. This confirms the proposition that using HSC with the newly proposed circular target produces a reliable estimation of displacement in the SPT components.

As shown in Fig. 14, the velocity data show excellent agreement between the SPT-HEMA and HSC systems across all N-values at both the anvil and sampler levels. The velocity profiles are consistent during the critical time window leading to peak displacement and representing the primary energy transfer phase. For lower N-values, the velocity profiles exhibit extended deceleration phases due to the longer penetration times. For higher N-values, the velocity profiles are shorter and more abrupt, reflecting quicker energy dissipation. The HSC system demonstrates slightly smoother stabilisation post-peak compared to the SPT-HEMA system, but both systems capture the key dynamics accurately.

The ETR data, as shown in Fig. 15, highlights the efficiency of energy transfer from the hammer to the sampler. Across all N-values, the peak ETR values align well between the SPT-HEMA and HSC systems at both the anvil and sampler levels. The ETR values rise rapidly during the time window corresponding to peak displacement and stabilise afterwards. For lower N-values, the energy transfer duration is longer due to larger penetration depths, while for higher N-values, the energy transfer is more concentrated. Although minor oscillations are observed in the SPT-HEMA energy data post-peak, particularly at higher N-values, the primary focus on the peak displacement window reveals a strong match between the two systems. The consistent ETR of 60 % ensures that these results represent a consistent energy input, eliminating variability due to differing hammer efficiencies. The uniform ETR of 60 % ensures that the observed variations are solely due to the dynamic differences associated with N-values rather than inconsistencies in energy input. These observations are in line with studies that have measured driving energy in SPT and various dynamic cone penetration tests, emphasizing the variability of energy transfer efficiency across different testing methods and soil conditions [23]. It can be highlighted that in the HSC system with a circular target, the ETR remains constant after reaching its peak. In contrast, in the sensor-based measurement system (SPT-HEMA), the ETR fluctuates due to the more considerable influence of the reflected tensile wave on subsequent wave propagation. The standard error (SE) of ETR at the anvil level was 0.32 % for SPT-HEMA and 0.11 % for HSC, while at the sampler level, it was 0.43 % for SPT-HEMA and 0.36 % for HSC. Both methods give reliable results for measuring ETR with lesser SE. However, the HSC system shows slightly more stable results. Additionally, the HSC integrated with circular targets can track the movements of the SPT component in all directions, which helps in better understanding the energy contributing to sampler penetration efficiency. It is important to note that the tests were performed in a controlled laboratory SPT model, and the results may vary under actual field conditions.

3.3. Summary and Conclusion

Image processing and non-contact measurement are among the leading research areas due to the development of AI/ML, which is comparatively less employed in geotechnical engineering, particularly SPT hammer energy measurement. In this study, for the first time, an effective circular target marking is integrated with a High-Speed Camera (HSC), and the energy delivered for the penetration of the SPT spoon sampler is estimated. Integrating a HSC system with circular target markers to overcome the limitations of conventional edge-based target markings on cylindrical SPT components and the conventional force and acceleration sensor-based methods. The proposed approach enables precise measurement of displacement, velocity, and Energy Transfer Ratio (ETR) as HSC with circular targets capture movements in all three

dimensions (X, Y, and Z coordinates). This approach also provides digital image data for a comprehensive understanding of the dynamic behaviour of critical SPT components.

Systematic, controlled SPT laboratory experiments were carried out in a full-scale model setup located at the Indian Institute of Science (IISc), Bangalore. The test was conducted on soil samples in the mould, with visual monitoring using HSC integrated with circular targets and sensor-based hammer energy measurement using SPT-HEMA, positioned just below the anvil and just above the split spoon sampler. Additionally, systematic SPT tests were conducted on soil samples of varying relative densities (\sim 15–90 %) within a controlled mould, ensuring different N-values (N = 5 to R) or penetration depth per blow (~60 to 3 mm), while maintaining a consistent input ETR of approximately ~60 %. The results demonstrate that the HSC system with circular targets successfully captures displacement, velocity, and ETR values comparable to those obtained from the SPT-HEMA system. Additionally, the manual vertical displacement measurement from the vernier-caliper pre- and post-SPT blow was in good match (within $\pm\,0.1$ mm) with the displacement obtained from the SPT-HEMA and HSC, further validating the accuracy of these measurement techniques.

The results demonstrate that the peak energy transfer coincides with the sensor-based peak values, emphasizing that this can be an alternate way to validate sensors. Further, lower N-values, representing greater penetration per blow, are associated with extended displacement durations and energy transfer phases, while higher N-values show shorter, concentrated energy dissipation. These trends are observed consistently at both the anvil and sampler levels, validating the reliability of the proposed system for capturing critical SPT dynamics.

The HSC system offers distinct advantages over traditional methods by isolating vertical movements, providing more precise energy and displacement measurements, and addressing complexities such as the multidirectional vibrations inherent in SPT. This can be extended to field conditions to measure energy without disturbing conventional testing.

Funding details

This work was supported by the SERB, DST, Govt. of India for the project "Development of correction factors for standard penetration test N values in India through energy measurement and field experiments – Step towards a reliable Liquefaction Potential Assessment" under Grant SERB/F/198/2017–18 dated 11/05/2017; and Dam Safety (Rehabilitation) Directorate, Central Water Commission for funding the "International Centre of Excellence in Dam Engineering" (ICoEDE) under the Dam Rehabilitation and Improvement Project (DRIP); Ministry of Jal Shakti (MoJS), Government of India for the project entitled "Integrated Investigation for Risk Assessment of the Dam" under grant R-24011/57/2023-Pen Riv Section-MOWR.

CRediT authorship contribution statement

M E Yadhunandan: Writing – original draft, Visualization, Validation, Software, Methodology, Investigation, Formal analysis, Data curation, Conceptualization. **Panjamani Anbazhagan:** Writing – review & editing, Visualization, Validation, Supervision, Resources, Project administration, Methodology, Funding acquisition, Conceptualization.

Declaration of competing interest

The authors declare that they have no known competing financial interests or personal relationships that could have appeared to influence the work reported in this paper.

Acknowledgements

The authors thank Mr. Silas and Mr. Sudhanshu, Research Scholar;

Dr. Tejas Murthy, Professor, Department of Civil Engineering, Indian Institute of Science, for their valuable contribution and input for the laboratory SPT Model setup testing.

Data availability

Data will be made available on request.

References

- [1] P. Anbazhagan, K. Ayush, M.E. Yadhunandan, K. Siriwanth, K. Suryanarayana, G. Sahodar, Effective use of SPT: hammer energy measurement and integrated subsurface investigation, Indian Geotech. J., 52 (5) (2022) 1079–1096, https://doi. org/10.1007/s40098-022-00609-z.
- [2] P. Anbazhagan, M.E. Yadhunandan, A. Kumar, Effects of hammer energy on borehole termination and SBC calculation through site-specific hammer energy measurement using SPT HEMA, Indian Geotech. J., 52 (2) (2022) 381–399, https://doi.org/10.1007/s40098-021-00582-z.
- [3] ASTM International, ASTM D4633-16 Standard Test Method for Energy Measurement for Dynamic Penetrometers, West Conshohocken, PA, USA., 2016. doi: 10.1520/D4633-16.
- [4] C.M. Santana, F.A.B. Danziger, B.R. Danziger, Energy measurement in the Brazilian SPT system, Soils Rocks 37 (3) (2014) 243–255, https://doi.org/10.28927/ SR.373243.
- [5] S.-N. Lee, B.-J. You, M.-S. Limb, S.-R. Oh, S.-S. Han, and S. H. Lee, "Visual measurement of pile penetration and rebound movement using a high-speed line-scan camera," In: Proceedings 2002 IEEE International Conference on Robotics and Automation (Cat. No.02CH37292), May 2002, pp. 4307–4312 vol.4. doi: 10.1109/ROBOT.2002.1014436.
- [6] M. Lim, S.R. Oh, B.-J. You, S.-S. Han, S.H. Lee, Visual precise measurement of pile rebound and penetration movement using a high-speed line-scan camera, Int. J. Control Autom. Syst. 4 (4) (2002) 341–346.
- [7] C. Lee, J.-S. Lee, S. An, W. Lee, Effect of secondary impacts on SPT rod energy and sampler penetration, J. Geotech. Geoenvironmental Eng., 136 (3) (2009) Sep, https://doi.org/10.1061/(ASCE)GT.1943-5606.0000236.
- [8] C. Lee, S. An, W. Lee, Real-time monitoring of SPT donut hammer motion and SPT energy transfer ratio using digital line-scan camera and pile driving analyzer, Acta Geotech. 9 (6) (2014) 959–968, https://doi.org/10.1007/s11440-012-0197-0.
- [9] E. H. Y. Sze, P. W. K. Chung, and E. K. L. Wong, "Energy transfer characteristics of standard penetration test using high-speed camera and instrumentations," In: *ResearchGate*, Sydney, Australia: Australian Geomechanics Society, Sydney, Australia, Jamuary 2022. [Online]. Available: https://www.researchgate.net/ publication/360560846_Energy_transfer_characteristics_of_standard_penetration_ test using high-speed camera and instrumentations.
- [10] K.H. Miller, An investigation of standard penetration test hammer efficiency through measurement of impact velocity and stress wave energy, University of British Columbia (2022), https://doi.org/10.14288/1.0413223.
- [11] Z. Zhang, "Flexible camera calibration by viewing a plane from unknown orientations," In: Proceedings of the Seventh IEEE International Conference on Computer Vision, Sep. 1999, pp. 666–673 vol.1. doi: 10.1109/ICCV.1999.791289.
- [12] S. P. Timoshenko, J. N. Goodier, and H. N. Abramson, "Theory of Elasticity (3rd ed.)," J. Appl. Mech. 37(3) (1970) 888, doi: 10.1115/1.3408648.
- [13] R.E. Kalman, A New Approach to Linear Filtering and Prediction Problems, J. Basic Eng., 82 (1) (Mar. 1960) 35–45, https://doi.org/10.1115/1.3662552.
- [14] G. Welch and G. Bishop, "An Introduction to the Kalman Filter," Univ. N. C. Chap. Hill, vol. Tech. Rep. TR 95-041, Jul. 2006.
- [15] D. Comaniciu, V. Ramesh, and P. Meer, "Real-time tracking of non-rigid objects using mean shift," In: Proceedings IEEE Conference on Computer Vision and Pattern Recognition. CVPR 2000 (Cat. No.PR00662), Jun. 2000, pp. 142–149 vol.2. doi: 10.1109/CVPR.2000.854761.
- [16] G. R. Bradski, "Real time face and object tracking as a component of a perceptual user interface," In: Proceedings Fourth IEEE Workshop on Applications of Computer Vision. WACV'98 (Cat. No.98EX201), Oct. 1998, pp. 214–219. doi: 10.1109/ ACV.1998.732882.
- [17] Bureau of Indian Standards, IS 2131:1981 (Reaffirmed 2021) Method for Standard Penetration Test for Soils, New Delhi, India., 2021. [Online]. Available: https:// www.scribd.com/document/735700898/ls-2131-1981-Reaffirmed2021-Standard-Penetration-Test.
- [18] J. Li, X. Xu, Z. Jiang, B. Jiang, Adaptive kalman filter for real-time visual object tracking based on autocovariance least square estimation, Appl. Sci. 14 (3) (2024), https://doi.org/10.3390/app14031045.
- [19] C. Beyan, A. Temizel, Adaptive mean-shift for automated multi object tracking, IET Comput. Vis., 6 (1) (2012) 1–12, https://doi.org/10.1049/iet-cvi.2011.0054.
- [20] J.A. Lukiantchuki, G.P. Bernardes, E.R. Esquivel, Energy Ratio (ER) for the standard penetration test based on measured field tests, Soils Rocks 2 (2017), https://doi.org/10.28927/SR.402077.
- [21] W.-T. Hong, S.Y. Kim, J.-S. Lee, Evaluation of driving energy transferred to split spoon sampler for accuracy improvement of standard penetration test,

- $\label{lem:measurement} \begin{tabular}{ll} Measurement 188 (2022) 110384, $https://doi.org/10.1016/j. \\ measurement. 2021. 110384. \end{tabular}$
- [22] E. Odebrecht, F. Schnaid, M.M. Rocha, G. de P., Bernardes, "Energy Efficiency for Standard Penetration Tests", J. Geotech. Geoenviron. Eng. 131 (10) (2005) https://doi.org/10.1061/(ASCE)1090-0241(2005)131:10(1252).
- [23] T. Matsumoto, L.T. Phan, A. Oshima, S. Shimono, Measurements of driving energy in SPT and various dynamic cone penetration tests, Soils Found. 55 (1) (2015) 201–212, https://doi.org/10.1016/j.sandf.2014.12.016.